Numerical optimization of cell colonization modelling inside scaffold for perfusion bioreactor: A multiscale model

T-K. Nguyen, Olivier Carpentier, Francine Monchau, F. Chai, Jean-Christophe Hornez, Ph. Hivart

Numerical optimization of cell colonization modelling inside scaffold for perfusion bioreactor: A multiscale model

T-K. Nguyen [a], O. Carpentier [a,*], F. Monchau [a], F. Chai [b], J.C. Hornez [c], P. Hivart [a]

[a] Univ. Artois, EA 4515, Laboratoire de Génie Civil et géo-Environnement (LGCgE), Béthune F-62400, France
[b] Univ. Lille, Inserm, CHU Lille, U1008 - Controlled Drug Delivery Systems and Biomaterials, Lille F-59000, France
[c] Laboratoire des Matériaux Céramiques et Procédés Associés (Université de Valenciennes et du Hainaut Cambresis), Bd. Charles de Gaulle, Maubeuge 59600, France

Part of clinically applicable bone graft substitutes are developed by using mechanical stimulation of flow-perfusion into cell-seeded scaffolds. The role of fluid flow is crucial in driving the nutrient to seeded cells and in stimulating cell colonization. A common numerical approach is to use a multiscale model to link some physical quantities (wall shear stress and inlet flow rate) that act at different scales. In this study, a multiscale model is developed in order to determine the optimal inlet flow rate to cultivate osteoblast-like cells seeded in a controlled macroporous biomaterial inside a perfusion bioreactor system. We focus particularly on the influence of Wall Shear Stress on cell colonization to predict cell colonization at the macroscale. Results obtained at the microscale are interpolated at the macroscale to determine the optimal flow rate. For a macroporous scaffold made of interconnected pores with pore diameters of above 350 μm and interconnection diameters of 150 μm, the model predicts a cell colonization of 325% after a 7-day-cell culture with a constant inlet flow rate of 0.69 mL · min^{-1}. Furthermore, the strength of this protocol is the possibility to adapt it to most porous biomaterials and dynamic cell culture systems.

1. Introduction

In the area of bone grafting, large bone deficits can arise from traumas, diseases, injuries or congenital defects. A bone graft substitutes is a scaffold in which cells are seeded. Cells need to grow to ensure a good densification of the grafts. Consequently, the bone graft substitutes need nutrients and waste removal. The static cell culture is the most common and the simplest way to develop bone graft substitutes[1–4]. However, the static cell culture has some drawbacks. First, the mechanical stimulation, an important parameter in cell growth [5,6], is neglected. Second, this method is not suitable for large bone substitute. Indeed, for large substitutes, nutrients cannot be delivered to the center of the scaffold and waste cannot be removed, leading to cell necrosis. One solution is the use of a device called a bioreactor that can generate dynamic cell culture [7–10]. This process provides both the necessary mechanical stimulation (pressure drop, shear stress) and the nutrient availability to cells [8,11]. There are numerous types of bioreactors. Direct perfusion bioreactors (DPB) efficiency is demonstrated in the enhancement of human cell growth and survival. These effects are mainly due to the constant renewal of the culture medium and the beneficial effect of fluids on cell activity [12–14].

Another important entity to study is the bone graft substitutes itself and its influence on cell culture. It would be unrealistic to give an exhaustive list of bone substitutes. In this paper, the study is limited to the case of a specific bioceramic. Due to the similar properties shared with human bones, bioceramics are nowadays widely used in bone grafting or in tissue engineering [15,16]. In particular, bioceramics based on calcium phosphate as hydroxyapatite (HA) or tricalcium phosphate (TCP) are highly developed due to their biocompatibility and osteoconductivity [17,18]. HA is used in this study for its law rate of biodegradation and therefore the stability of the macroporous structure of scaffold. An increasing number of studies provide a generous amount of details about their applications in bone grafting [19–23].

Cell culture takes place in a saturated bioceramic with culture medium. The biological fluid flows through the pores of the bioceramic material and induces a specific pressure on cells called Wall Shear Stress (WSS). This stress is a fundamental parameter affecting cell growth and survival [24]. In this study, wall shear stress is estimated on the walls of the scaffold. Wall Shear Stress depends on fluid velocity and this velocity is linked to the flow rate selected on the DPB. If the inlet flow rate is too low, mass transfer limitations cannot be overcome and nutrients cannot be present at the

* Corresponding author.
E-mail address: olivier.carpentier@univ-artois.fr (O. Carpentier).

Nomenclature

Roman symbols

c_m	Michaelis-Menten constant ($mol \cdot m^{-3}$)
c_{O2}	Dioxygen concentration ($mol \cdot m^{-3}$)
d_i	Interconnection diameter (μm)
d_s	Pore diameter (μm)
D_x	Diffusion coefficient of x specie ($cm^2 \cdot s^{-1}$)
K	Permeability (m^2)
p or P	Pressure (Pa)
Q	Flow rate ($mL \cdot min^{-1}$)
Q_m	Max velocity of O_2 consumption ($mol \cdot cell^{-1} \cdot s^{-1}$)
R_c	Colonization rate (s^{-1})
R_d	Death rate (s^{-1})
u	Fluid velocity ($mm \cdot s^{-1}$)
u_D	Darcy velocity ($mm \cdot s^{-1}$)

Greek symbols

μ	Dynamic viscosity ($Pa \cdot s$)
ρ	Density of fluid ($kg \cdot m^3$)
ρ_{cell}	Cell Density inside a scaffold ($cell \cdot ml^{-1}$)
ρ_{max}	Maximum of ρ_{cell} inside a scaffold ($cell \cdot ml^{-1}$)
τ	Wall shear stress (Pa)
ε	porosity

centre of the scaffold. If the inlet flow rate is too high, the velocity inside the pores is consequently also too high and the seeded cells in the scaffold could be dead or detached [25].

Finally, another important point to be studied is the oxygen supply for cell culture. A low oxygen concentration could be a limiting effect on cell culture. The biological fluid contains dioxygen that flows inside the porous material. Therefore, fluid mechanics equations at the macroscale must be coupled with diffusion equations and oxygen consumption equations to ensure a whole distribution of nutrients inside the porous media. Because of the process of perfusion into a scaffold takes too much time during the in vitro experiment and due to the fact that the manipulations are complex and the process takes time and is expensive. The optimal flow rate for cell proliferation is very difficult to identify through trial-and-error.

In this paper, and in order to save time in cell culture optimization inside bioceramics, a numerical method to identify the optimal flow rate is presented. The numerical method is based on a multiscale approach and Computational Fluid Dynamics (CFD). The multiscale approach is a common approach in CFD studies because in most cases calculus stations have not enough computational capacity to solve the entire problem from a complete microscale description. Our numerical protocol is composed of six steps. Each step can be treated separately and provides key numerical physical quantities (i.e local velocities, global Darcy velocities and wall shear stress). Therefore, each step is not an integral part of a global method, but part of a stack of numerical methods that can be separately improved or treated on various calculus stations without disrupting the operating protocol. Another advantage of this protocol is that it can be adapted to various kinds of scaffolds (geometry, porosity) submitted to dynamic cell culture.

The present work focuses on dynamic cell culture into direct perfusion bioreactor . A scaffold commonly used as bone graft substitutes, with a controlled porosity, has therefore been deliberately chosen for the study [26]. This scaffold is used because of its good properties in term of cells colonization on the surface, of nutrient supply to cells and of waste evacuation. The aim of this research is to determine the optimal flow rate of a direct perfusion bioreactor in order to enhanced cell proliferation and to improve an upcoming bone reconstruction.

2. Materials and methods

In our works, we consider an entire system used to carry out dynamic cell culture. The system is so composed of:

- A DPB for which the flow rate of biological fluid can be adjusted.
- Macroporous bioceramics defined at the microscale by pores arrangement (pore size, interconnection diameter, structure) and at the macroscale by the global size and shape of the scaffold.
- A biological fluid considered as an incompressible Newtonian fluid.
- Target cells for bone substitute.

These elements are those taken into account to carry out numerical simulations.

To understand the mechanical behaviour of cell growth into a bioceramic scaffold submitted to dynamic cell culture, a Computational Fluid Dynamic (CFD) analysis on two scales is performed. A model of spherical packaging and REV was implemented using Python (Python Software Foundation. Python Language Reference, version 2.7) and its Numpy and Scipy modules [27]. At the Representative Elementary Volume (REV) scale (microscale) the mechanical stress and WSS distribution identification was performed using finite volume method (ANSYS-Fluent). ANSYS-Fluent code is used because of its advantage in memory usage and solution speed especially when working with common calculus station. Then, the statistical analysis necessary to identify the optimal range of growth stress is developed into a Python code. Finally, velocity and stress into the macroscopic bioceramic material is computed thanks to a finite element analysis with COMSOL, and more specifically the mathematics module that allows users to implement custom model. The mathematics module is so used to solve both equations based on fluid mechanics and on biology in an easier fashion than with a finite volume method. Concerning the scaffold, a classic biodegradable porous material with 100% open pores architecture is used [26].

Concerning the Wall Shear Stress at the pores scale (microscale) is calculated inside a REV. The REV is composed of a fluid part and a solid part, represented by a dozen of spherical interconnected pores. REV is built with a random distribution in order to imitate the real pore distribution of manufactured bioceramics made at the LMCPA (Laboratoire des Matériaux Céramiques et Procédés Associés, Biocetis® product of type HA40-P090825). The shear stress distribution is evaluated as a function of inlet flow rate (Q). The model used at the microscale is based on Navier–Stokes equation for an incompressible Newtonian fluid. Thanks to a previous study [28] we can give an expression of Darcy velocity from a Wall Shear Stress distribution and the evaluation of permeability into porous bioceramics with spherical interconnected pores. The published literature gives the optimal range of values of Wall Shear Stress that cells need for their growth, e.g values of WSS between 5e-3 Pa and 1e-2 Pa [29–34]. These studies are all numerical ones. Indeed, with the exception of Doppler Optical Coherence Tomography (DOCT), and even if improvements on experimental methods used to measure the wall shear stress are tangible, there are no currently available accurate experimental methods able to determine the wall shear stress on bioceramics in connection with our study case (at least to our knowledge). The DOCT was used with success on porous scaffold with a mean Wall Shear Stress between 3.8e-2 and 4.9e-2 Pa [35] but without any analysis of Wall Shear Stress on cell necrosis, so we cannot use experimental data to target the optimal range of Wall Shear Stress . μPIV methods are also in constant development and seem to be suitable for the determination of velocities. Furthermore, the correlations between experimental and numerical data are good [36]. In fact, with the μPIV

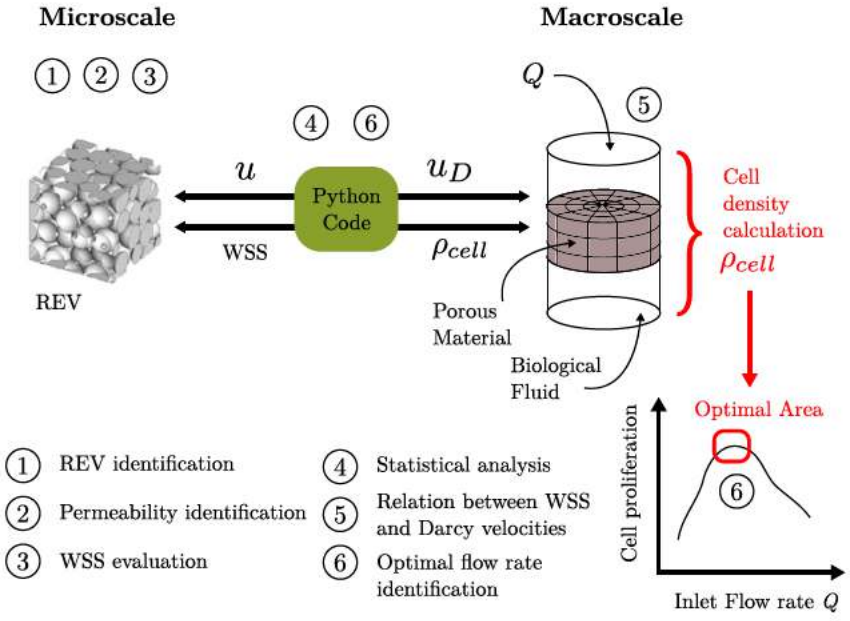

Fig. 1. Multiscale model and steps to identify the optimal flow rate.

methods, Wall Shear Stress is not directly measured but can be estimated from velocity fields, as with the numerical methods.

Before describing the detailed numerical protocol that allow us to estimate the cell proliferation in a bioceramic, we give to the reader a brief explanation of the relationship between the wall shear stress and the inlet flow rate (Fig. 1). The overall idea is to start from the Dupuit–Forcheimer relation (Eq. (3)) in which the local velocities u and the global velocity U_D in a given volume are expressed. So, with enough known parameters (e.g the permeability and geometry of a porous media), information at the microscale can be connected to information at the macroscale. Then, if the global velocity U_D is substituted with the inlet flow rate Q ($U_D = QL/A$, L is the length of porous media and A its area) the relationship between the inlet flow rate Q and the local velocities u is established. Moreover at the microscale the wall shear stress is evaluated by solving the Navier–Stokes equations (Eqs. (4) and (5)) in a representative elementary volume (REV). The relationship between the wall shear stress and the inlet flow rate is not obvious. In order to make it easier, a statistical log-normal function that describe the stress distribution is introduced. This statistical function is expressed with the local velocities u and, by identification, can be also expressed as a function of inlet flow rate (Eq. (18)). Finally, fluid mechanics equation are crossed with biologicals ones for the estimation of the cell proliferation.

So, according to the literature, inside this optimal range of values of Wall Shear Stress (5e-3 Pa and 1e-2 Pa) we target a smaller one to optimize the prediction of cell growth. The identification of this smaller range of value is detailed in Section 2.4. In the second phase, the bioreactor and the entire scaffold (bioceramics) are modelled. The cell colonization is studied thanks to both the Navier-Stokes equation (outside of the scaffold) and a Darcy-based formulation (inside the scaffold) to compute velocities and stress. Additional equations are also required in order to describe the nutrient consumption by the cells. The computational modelling is then carried out with some values of inlet flow rate and cell colonization can therefore be estimated.

2.1. REV identification - Microscale

Identification of the REV is the first step to allow us to establish a connection between the two scales (micro and macro).

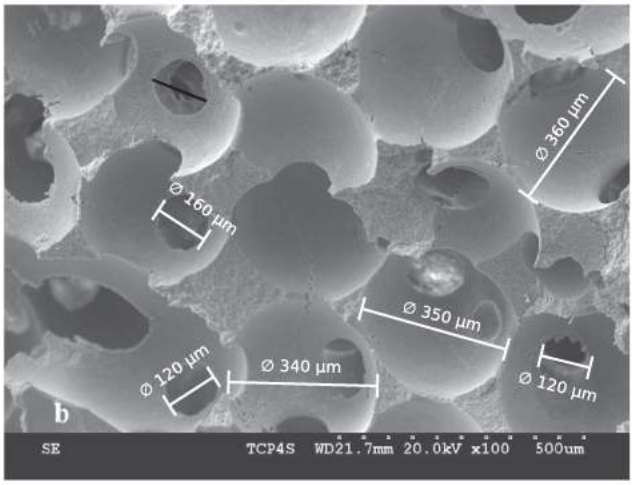

Fig. 2. SEM imaging of porous scaffold used as a reference for our numerical studies. Scaffold have average diameters of 350 µm and average diameters of interconnection of 150 µm.

Works are carried out into a virtual and tangential spheres package random assembly. Spheres are then interconnected by increasing the spheres' radius. To stay as close as possible to real bioceramics used in *in vitro* experiments [26] (Fig. 2), mean value of sphere diameter d_s and interconnection diameter d_i are used here ($d_s = 350\,\mu m$, and $d_i = 150\,\mu m$). The following steps are used to make the REV identification.

1. Virtual random assembly of 1000 spheres into a reference volume V_∞.
2. At the centre of the reference volume, an elementary volume V_0 grows from 0 to V_{max} with $V_{max} > V_\infty$. Into this elementary volume there is a fluid fraction Φ_f and a solid fraction Φ_s. We can therefore express the solid volume V_s of V_0, $V_s = \Phi_s \cdot V_0$.
3. The porosity of V_0 is calculated by $\varepsilon_0 = 1 - \frac{V_s}{V_0}$.
4. The procedure is iterative. For each step V_0 growths and another elementary volume is calculated: $V_0^i = V_0^{i-1} + dV$. The value of DV is chosen as a single pore volume to ensure a vari-

Table 1
Wall Shear Stress (WSS) effects on cell culture estimated by numerical models found in literature. (a) Lattice–Boltzmann Method, (b) Finite Element Method, (c) Finite Volume Method.

WSS	Effect	Method	Structure	References
1×10^{-5} Pa	Increase cell growth	LBM[a]	Fibrous Matrice	[29]
5×10^{-5} Pa	Increase cell growth	LBM[a]	Spherical pores	[30]
2.5×10^{-4} Pa	Increase cell growth	FVM[c]	Spherical pores	[31]
5×10^{-3} Pa	Increase cell growth	FEM[b]	Spherical pores	[32],[33]
1.1×10^{-2} Pa	Increase cell growth	FEM[b]	Spherical pores	[33]
1.5×10^{-2} Pa	Cell growth inhibition	FEM[b]	Spherical pores	[33]
4×10^{-2} Pa	Cell necrosis	FEM[b]	Foam from CT-Scan	[34]
5.7×10^{-2} Pa	Cell necrosis	LBM[a]	Spherical pores	[30]

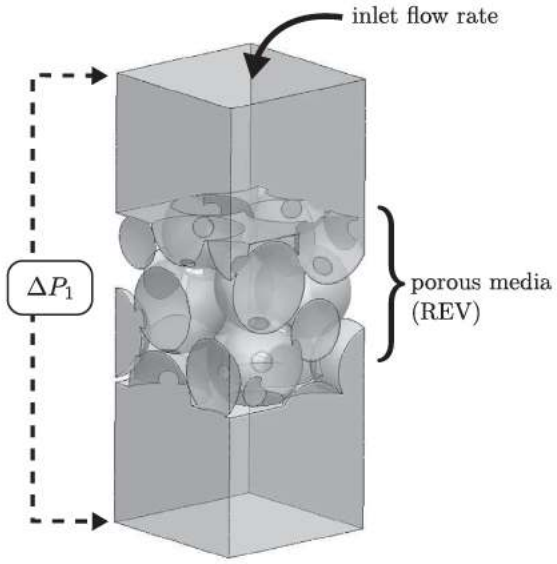

Fig. 3. An example of REV with random structure used for numerical identification of permeability.

ation small enough to reach the porosity level with accuracy. Another porosity ε_0^i is calculated and the variation of porosity between two steps is calculated: $\Delta\varepsilon_0^i = \mid \varepsilon_0^i - \varepsilon_0^{i-1} \mid$.

5. When $\Delta\varepsilon_0^i < Tol$. the REV is identified.

For $Tol = 5e-3$ a REV of above $8\,\text{mm}^3$ is identified that corresponds to a porosity $\varepsilon_0 = 0.71$ and about 12 interconnected spheres.

2.2. Permeability Identification - Microscale

This work is based on a virtual representation of the experimental test of the measurement of pressure losses. The full method is detailed in a previous work [28] and the important steps are summed up here.

We consider the following expression of Darcy Law (Eq. (1)):

$$\frac{QL}{A} = U_D = -\frac{K}{\mu}\nabla P \tag{1}$$

With U_D the Darcy velocity, Q the inlet flow rate, L the length of the REV, A the area of the REV, K the permeability and μ the dynamic viscosity.

A virtual current tube is then modelled. The pressure difference ΔP_2 between inlet pressure and outlet pressure is measured into this tube. Then a porous REV geometry is placed into the tube and the pressure difference $\Delta P_1$is calculated (Fig. 3). Pressure losses are simply expressed by $\Delta P = \Delta P_2 - \Delta P_1$. As the Darcy velocity u_D and the pressure losses ΔP are known, for a given direction i the permeability K_i can be identified. For non-isotropic medium (like fibrous medium), the porous REV can be oriented in other directions to identify the complete permeability matrix. In our case, the porous architecture is considered as isotropic. The following options are inserted into ANSYS-Fluent to carry out the numerical simulation.

- Steady laminar analysis.
- Incompressible fluid.
- Fluid is water at 37 °C.
- No slip wall conditions.
- Flow rate inlet imposed.

We notice that to ensure a Stokes flow ($Re < 1$) the Darcy velocity must not exceed $1.9\,\text{mm} \cdot \text{s}^{-1}$.

2.3. Wall Shear stress evaluation - Microscale

When the permeability K of a porous medium is known, a connection can be established between a Darcy velocity and a pressure (Eq. (1)). Darcy velocity is considered as constant into the REV. The aim of this part of the protocol is to compute τ, the Wall Shear Stress (WSS), as a function of a given inlet flow rate Q. WSS targeted values are those effective at good cell colonization. Even though these Wall Shear Stress values are scattered, there is a broad consensus of about the maximal value of τ beyond which cells are necrotized (Table 1).

Due to geometrical variations inside the scaffold, the WSS cannot be a constant. The computed Wall Shear Stress τ is therefore not a value but a range of values in which an optimal Wall Shear Stress $\tau^\star$ exists that correspond to an optimal cell growth. For a given inlet flow rate Q, the purpose is to identify the greatest occurrence. We consider a value of WSS as good as it induce an increase of cell growth lik the occurrence of $\tau^\star$ inside the range of WSS values.

The following steps describe how to perform the WSS evaluation inside the REV.

1. Build geometry and mesh of the REV.
   - Unstructured mesh.
   - Tetrahedral elements.
2. Solve Navier-Stokes equations with CFD and the following parameters.
   - Flow: Stationary and Laminar flow.
   - Compressibility: Incompressible fluid.
   - Wall condition: No slip.
   - Fluid part on side of porous media: periodic boundary condition.
   - Inlet condition: Flow rate between 0 and 10 $\text{mL} \cdot \text{min}^{-1}$.
   - Outlet condition: Gauge pressure set to zero.
   - Pressure-velocity coupling: SIMPLE Algorithm.
   - Convergence criteria: 1×10^{-6} for all equations.
3. Velocity field computation.
4. Results post-processing and computation of WSS distribution on pores.

A sensitivity analysis on maximal Wall Shear Stress is carried out to confirm the grid independence to main variables.

2.4. Statistical analysis - Microscale

The statistical analysis is necessary to identify the process of identifying the optimal range of WSS for cell growth which is implemented in Python code using Numpy and Scipy modules. All the data from the CFD computation are stored into a table that contains mesh elements, their volumes and surfaces and the associated Wall Shear Stress . WSS and elements surfaces are extracted from elements that correspond to pores surfaces. For a given element, the Wall Shear Stress contribution is just computed as follows (Eq. (2)).

$$P_\tau^e[\%] = \frac{S_\tau^e}{S_i} \times 100 \tag{2}$$

Where e is a volume element, S_τ^e the value of the surface of the volume element at the interface between solid phase and fluid phase, S_i the value of the total surface of the interface and so P_τ^e the percentage of a computed Wall Shear Stress corresponding to the surface element.

The first step is to plot a histogram of the percentage of surface experiencing a particular range of Wall Shear Stress range as a function of the inlet flow rate. Most of the data can be represented by statistical functions such as Log-Normal function for example. The aim of this step is to identify a function from several points to describe the entire distribution of Wall Shear Stress for a given flow rate.

With the existing calculus stations, the identification of the exact value of $\tau^\star$ requires a prohibitive computational cost. Even the use of a sliding window analysis remains a prohibitively costly solution considering the vast amount of data. So, an initial range of Wall Shear Stress (from 1e-5 Pa to 1e-2 Pa) could be subdivided into smaller ranges where statistical analysis are carried out.

More specifically, by inversion, for each range of Wall Shear Stress , the optimal flow rate, i.e. the flow rate for which the distribution of a given range of Wall Shear Stress is maximized, can be easily identified.

When the kind of statistical function is known, parameters need to be identified (Fig. 1). There are numerous algorithms to identity these parameters (direct inversion when possible, genetic algorithm, Simplex, etc.). For this analysis a Simplex algorithm is be used to fit the function [37]. With the parameters known, a distribution function of Wall Shear Stress related to inlet flow rate Q is established. The next step is to link the inlet flow rate Q and Darcy velocities inside the REV to establish a connection between the microscale and the macroscale.

2.5. Relation between WSS and Darcy velocities - From microscale to macroscale

The advantage of understanding the physical laws inside a REV is to make an assembly of several REV that will both describe any kind of geometry and address the issue of fluid mechanics problem. If an element, as in finite element method, is considered as a REV, physical quantities (like velocities) inside this element are represented by a mean value of the physical quantities. In our analysis, a relation between Wall Shear Stress and flow rate Q and then between Wall Shear Stress and Darcy velocities is established. Darcy velocities are calculated from Dupuit–Forcheimer relation. The plot of Darcy velocities as a function of inlet flow rate gives us a function like $u_D = f(Q)$. In most cases, the function f can be written as $f(Q) = a \cdot Q$ with a a real number (Eq. (3)). Consequently, Q can be replaced by u_D in the statistical equation identified in the previous step.

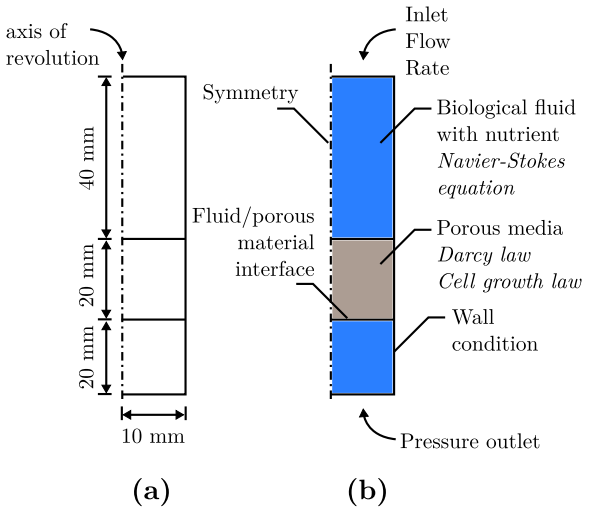

Fig. 4. Details of the macroscopic axisymmetric model: (a) dimensions (b) Boundary and numerical study conditions.

$$a \cdot Q = \underbrace{u_D = \varepsilon \int_V u \, \mathrm{d}V}_{tnDupuit-Forcheimerrelation} \tag{3}$$

Thanks to the relation between Q and u_D and therefore between u_D and the Wall Shear Stress , it is possible to calculate the percentage of surface on which τ is greater than 1.5×10^{-2} Pa for a given inlet flow rate Q. It should be recalled that the chosen value of τ corresponds to a value over which cells are necrotized. The percentage that represents an acceptable threshold limit is arbitrarily chosen. The symbolic value of 50% of living cells is chosen, i.e. the inlet flow rate must not induce more than 50% of necrotized cells [16] and so the WSS must be not greater than 1.5e-2 Pa for half of the total pores surfaces (Table 1).

In order to know the critical inlet flow rate, the percentage of necrotized cells as a function of inlet flow rate must be plotted. Then, thanks to the previous equation (Eq. (3)), the critical value of Darcy velocity in the macroscopic study can be found. In short, the protocol is the following.

1. Calculation of Darcy velocities u_D in a REV for a given inlet flow rate Q (Eqs. (1) and (3)).
2. Calculation of parameters of the correlation function f for $u_D = f(Q)$.
3. The threshold of cell necrosis is chosen.
4. Identification of critical inlet flow rate Q.
5. Identification of critical Darcy velocity.

At the end of this step, the relation between the inlet flow rate and the Wall Shear Stress is established. At the macroscale, the scaffold geometry can be represented and the fluid mechanics problem can be solved. However, an equation that describes cells growth and necrosis is needed to find the optimal flow rate.

2.6. Optimal flow rate identification - Macroscale

In this final step, two complementary approaches must be carried out.

- Cells must receive the adequate stress.
- Cells must be fed.

The macroscopic model used (Fig. 4) comprises a fluid part and a porous material (a cylinder in our case). Because of the symmetries on geometries and boundaries conditions an axisymmetric

Table 2
Parameter table for the macroscopic study.

Variable	Value	Units	Explanation	References
$\varepsilon(t_0)$	0.71		Porosity at initial time	[26]
ρ	893	$kg \cdot m^3$	Density of biological fluid	[42]
μ	8.3×10^{-4}	$Pa \cdot s$	Dynamic viscosity	[42,43]
D_{O2}	1.4×10^{-5}	$cm^2 \cdot s^{-1}$	Dioxygen diffusion	[39]
$c_{O2}(t_0)$	0.199	$mol \cdot m^{-3}$	Dioxygen concentration at initial time	[38,44]
c_m	0.0058	$mol \cdot m^{-3}$	Michaelis Constant	[39]
Q_m	16.3×10^{-18}	$mol \cdot cell^{-1} \cdot s^{-1}$	Maximum velocity of dioxygen consumption by a cell	[45,46]
ρ_c	1072–1086	$kg \cdot m^3$	Specific density of a cell	[47,48]
V_c	2.801×10^{-18}	m^3	Volume of a cell	[49]
$\rho_{cell}(t_0)$	3×10^6	$cell \cdot ml^{-1}$	Initial cell density value	
F_c^{max}	1.337×10^{-6}	s^{-1}	Maximum of cell colonization	[3]
K_c	0.154		Contois Parameter	[42]
R_d	3.85×10^{-7}	s^{-1}	Rate of cell death	[42]
ρ_{max}	5×10^{14}	$cell \cdot m^{-3}$	Maximum of cell density inside the scaffold	[50,51]
D_{cell}	5×10^{-9}	$cm^2 \cdot s^{-1}$	Coefficient of cell diffusion into the scaffold	[51]

model is used. The mesh is structured and composed of quadrangle elements. Sensitivity analysis based on optimal flow rate evaluation is carried out to confirm the grid independence to numerical solutions. Fluid part contains nutrients to be brought to the cells. In our case, the nutrient is dioxygen. The porous material is constituted of a fluid part that contains cells to be fed and a solid part in which the Wall Shear Stress is calculated. In the fluid part, i.e. outside the porous material, Navier-Stokes equations and an evolution of concentration of dioxygen law are used (Eqs. (4)–(6)).

$$\nabla \cdot \vec{u} = 0 \tag{4}$$

$$\rho\left[\frac{\partial \vec{u}}{\partial t} + (\vec{u} \cdot \nabla)\vec{u}\right] = \rho\vec{g} - \nabla p + \mu \Delta \vec{u} \tag{5}$$

$$\frac{\partial c_{O2}}{\partial t} = -(\nabla \cdot c_{O2}\vec{u}) + \nabla \cdot (D_{O2}\nabla c_{O2}) \tag{6}$$

Where u is velocity in the fluid part, ρ the density of the biological fluid, p the pressure, μ the dynamic viscosity of the biological fluid, c_{O2} the dioxygen concentration and D_{O2} the diffusion coefficient of dioxygen.

Inside the scaffold, four equations (Eqs. (7)–(9)) are used to describe the fluid incompressibility, the Darcy law, the dioxygen consumption and the evolution of cell density.

$$\nabla \cdot \vec{u_D} = 0 \tag{7}$$

$$\nabla p = \frac{\mu}{K} u_D \tag{8}$$

$$\frac{\partial c_{O2}}{\partial t} = -(\nabla \cdot c_{O2}\vec{u_D}) + \nabla \cdot (D_{e-O2}\nabla c_{O2}) + R_{O2}$$

$$\frac{\partial \rho_{cell}}{\partial t} = (R_c - R_d)\rho_{cell}\left(1 - \frac{\rho_{cell}}{\rho_{max}}\right) - \nabla(D_{cell}\nabla\rho_{cell}) \tag{9}$$

Where u_D is the Darcy velocity, K the permeability of the scaffold, D_{e-O2} the effective diffusion coefficient of dioxygen, R_{O2} the consumption velocity of nutrient by cells, ρ_{cell} the cell density, D_{cell} the coefficient of cell diffusion in the scaffold, R_c the rate of cell growth, R_d the apoptosis rate and ρ_{max} the maximum value of cell density that can be reach in the scaffold. The effective diffusion D_{e-O2} is given by the Maxwell equation (Eq. (10)) [38].

$$D_{e-O2} = D_{O2}\frac{2\varepsilon}{3-\varepsilon} \tag{10}$$

Dioxygen consumption must satisfy the Michaelis–Menten kinetics equation of (Eq. (11)) [38–40].

$$R_{O2} = -\rho_{cell} \times \frac{c_{O2}}{c_m + c_{O2}} Q_m \tag{11}$$

where c_m is the Michaelis constant and Q_m the maximum velocity of dioxygen consumption by a cell.

The main work is to describe R_c, a function that contains the relation between WSS and cell colonization. Without dioxygen there is no colonization. However, there is also a cell colonization induced by dioxygen only without WSS. So R_c can be written as follows (Eq. (12)).

$$R_c = F(c_{O2}) + F(WSS)F(c_{O2}) \tag{12}$$

$F(c_{O2})$ is already described by the Contois equation (Eq. (13)) [41], [40].

$$F(c_{O2}) = F_c^{max}\frac{c_{O2}}{K_c\ \rho_{cell}\ V_c\ \rho_c + c_{O2}} \tag{13}$$

where F_c^{max} is the maximum of cell colonization due to dioxygen consumption, K_c the Contois parameter, ρ_c the specific density of one cell and V_c the volume of one cell.

Then, the $F(WSS)$ function can be described in three ranges of values. Beside a value of WSS (fewer than 1e-5 Pa), there is no cell colonization. Inside the optimal range of stress, the cell colonization can be described by a statistical function $f(Q)$ adjusted by the percentage k of cells that received the optimal stress. If the WSS is too important (greater than 4e-2 Pa), the cells die and $F(WSS)$ must be negative. So, from Eq. (12) R_c it can be written as (Eq. (14)).

$$R_c = [1 + F(WSS)] \cdot F(c_{O2}) = [G\{1 + f(Q)\}] \cdot F(c_{O2}) \tag{14}$$

where G is a function that takes the value of 1 when u_D is less than u_{Dmax} and a quick transition to the value of -1 otherwise (Eq. (15)).

$$G = -\left[\tanh(10^5 \cdot (u_D - u_{Dmax})) + 1\right] \tag{15}$$

Finally, solving this problem needs a last step, i.e. to take into account the evolution of permeability of the scaffold as a function of cell density. In a previous work [28], a relation between porosity and permeability has been established (Eq. (16)) thanks to the following Carman-Kozeny equation.

$$K(\varepsilon, t) = 9.956 \times 10^{-11}\frac{\varepsilon(t)^3}{(1-\varepsilon(t))^2} \tag{16}$$

Using a Taylor series expansion, the porosity of the scaffold as a function of time can be written as follow (Eq. (17)).

$$\varepsilon(t) = \varepsilon(t_0)\exp\left(-\frac{\rho_{cell}(t) \cdot V_c}{\varepsilon(t_0)}\right) \tag{17}$$

Parameters used for the computational modelling are referenced in Table 2.

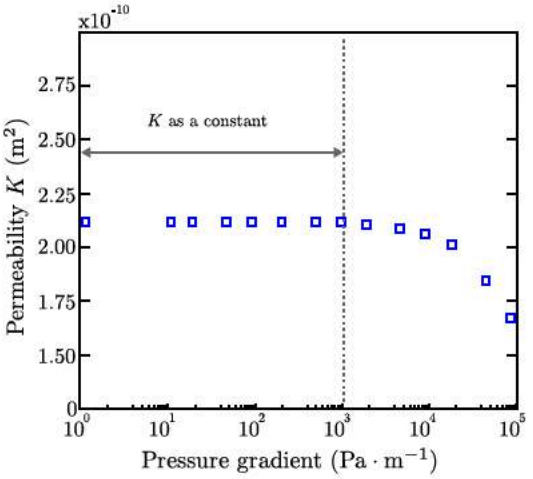

Fig. 5. Permeability K of the scaffold as a function on pressure gradient for random interconnected pores with porosity $\varepsilon = 0.71$.

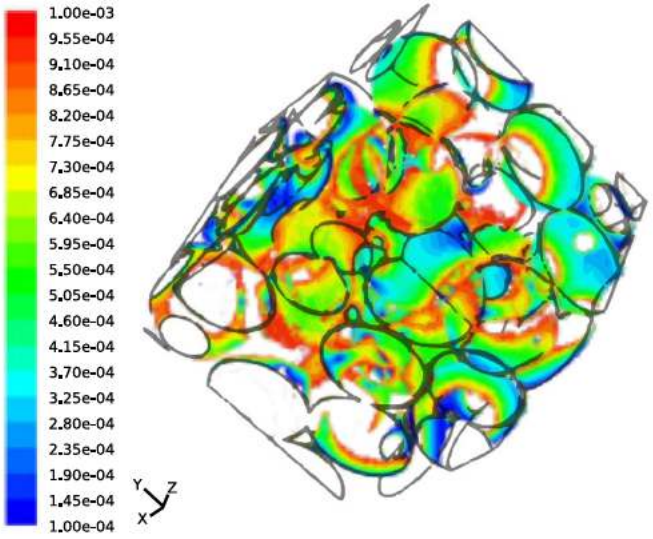

Fig. 6. Distribution of wall shear stress values τ in the REV between 10^{-4} Pa and 10^{-3} Pa.

3. Results

All the results presented in this part are given for a porous media composed of interconnected pores and a mean value of sphere diameter $d_s = 350\ \mu$m and interconnection diameter $d_i = 150\ \mu$m. However,the protocol described in the previous part allows us to work with a large range of porous media (structured and unstructured).

REV identification is the preliminary step (2.1). The REV allows us to build a 3D geometrical model useful to identify the permeability of our bioceramic material. The permeability is a parameter that depends on pressure gradient [52] (i.e. velocities or inlet flow rate) imposed on boundaries of the model. Results show (Fig. 5) that permeability can be considered as a constant for a pressure gradient less than 1000 Pa $\cdot$ m^{-1}. In our study the pressure gradient is about 20 Pa $\cdot$ m^{-1} and the hypothesis of a constant permeability without cell colonization is numerically validated. We identified $K = 2.1 \times 10^{-10}$ m^2.

The following step is to identify the statistical distribution of the Wall Shear Stress thanks at the microscale study. The Fig. 6 shows the WSS distribution for a given range of pressure. The data represented in Fig. 6 is known for each numerical element and each stress computed on an numerical element can be stored into a comma-separated value file. For various inlet flow rates, a percentage of distribution of a given range of Wall Shear Stress as a function of inlet flow rate Q can be plotted. For example, for two values τ_1 and τ_2 inside the initial range, and for a given inlet flow rate, the percentage of Wall Shear Stress computed seen on histogram is the highest. This operation could be carried out again inside τ_1 and τ_2 to identify a smaller range and so on. In this study, in order to avoid inducing prohibitive calculus cost, two loops are implemented (Fig. 7).

As a result, an optimal range of Wall Shear Stress value is identified, and, into this specific range, the computation of Wall Shear Stress distribution for all flow rates is not needed. In order to estimate the optimal range of values of WSS for cell growth, some computations are needed. A sliding window is used inside the initial range of WSS (from 1e-5 Pa to 1e-2Pa). As to determine the exact optimal value of WSS induces a prohibitive computational cost, the numerical procedure by successive approximations appears to be a good compromise between accuracy and computing cost. The points representing numerical simulation seems to be fitted by a log-normal function like the Eq. (18).

$$f(Q) = \frac{1}{aQc\sqrt{2\pi}} \exp\left[-\left(\frac{\ln(aQ) - b}{c\sqrt{2}}\right)^2\right] \tag{18}$$

where a, b and c are parameters identified by a SIMPLEX algorithm. In this example, the identified parameters of Eq. (18) are $a = 171.9613$, $b = 0.8983$ and $c = 0.8405$.

Then, at pores size (microscale), the Darcy velocity u_D is computed from Eq. (3) for various flow rates Q. The purpose here is to find a relation between u_D and Q in order to replace u_D by Q in the log-normal function (Eq. (18)) and directly use the results of macroscale analysis (i.e. Darcy velocity and homogenized pressure) to predict cell colonization (Eq. (14)). The Fig. 8 shows a linear relation between the Darcy velocity and the flow rate.

Finally, the macroscale analysis: during this step which takes into account how the fluid flows through the macroporous scaffold and how nutrients can be supplied to the cells, it is possible, with numerous numerical simulations to identify the optimal inlet flow rate. As an example, Fig. 9 shows the distribution of dioxygen concentration for a constant inlet flow rate $Q = 0.69$ mL $\cdot$ min^{-1}. A stratification is observed giving us reasons to assume that cell density is more important on the top of the scaffold. At the ending time (seven days of cell culture modelling), the cell density evolution can be calculated.

To be accurate, here are the different steps to obtain the optimal flow rate. At first, 6 ranges of Wall Shear Stress are studied (from $[10^{-5}; 5 \times 10^{-5}]$ to $[5 \times 10^{-3}; 10^{-2}]$ Pa) for 20 flow rates (from 10^{-3} to 10 mL $\cdot$ min^{-1}). Data analysis is carried out to focus on more specific ranges of WSS and flow rates. Due to the cost of numerical simulations only the two best flow rates (0.27 and 0.69 mL $\cdot$ min^{-1}) and two most common flow rates (1.0 and 3.0 mL $\cdot$ min^{-1}) are kept for the fine analysis. After 120 simulations, the range of $[10^{-4.1}; 10^{-2.3}]$ Pa and the four flow rates are studied for an optimized cell colonization. Then, 64 new simulations are carried out to accurately localize the optimal range of Wall Shear Stress for the given four flow rates previously identified. A new data analysis allows us to determine the optimal range of Wall Shear Stress . As the model used is axisymmetric, it is impossible to evaluate the exact number of cells at the end of the simulation but it remains possible to evaluate the growth rate of cell density. Fig. 10 represents the growth rate for the four identified flow rates. The best result is given for a flow rate $Q = 0.69$ mL $\cdot$ min^{-1} that corresponds to a growth rate of above 325% for a 7-day-cell culture and an optimal flow rate range of $[10^{-3.3}; 10^{-3.0}$mL $\cdot$ min$^{-1}]$.

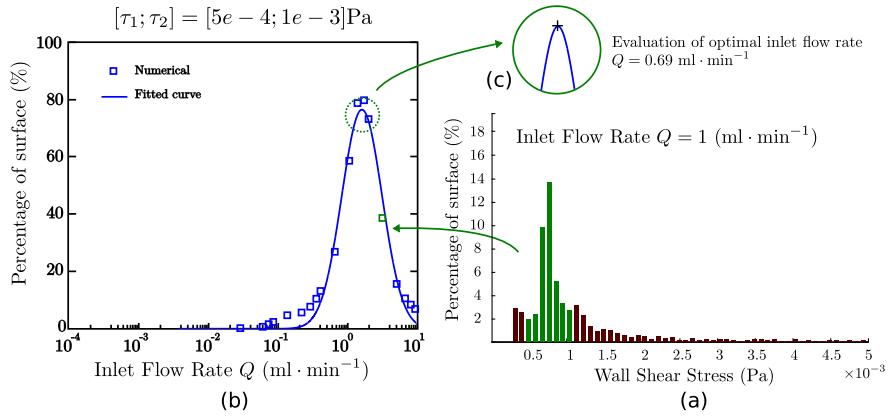

Fig. 7. (a) Histogram of WSS distribution for a given inlet flow rate, (b) Comparison between numerical data and log-normal function fitted, (c) Maximum of distribution and optimal inlet flow rate estimation.

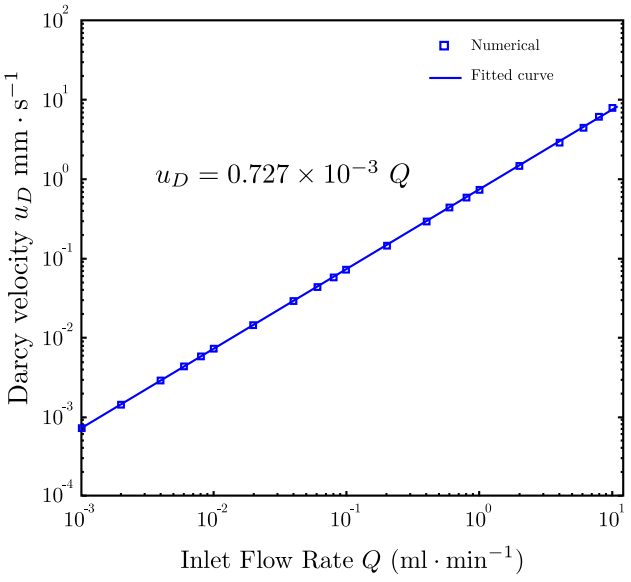

Fig. 8. Darcy velocity calculated in the REV as a function of flow rate Q.

Table 3
Synthesis of identified parameters with the numerical protocol for a bioceramic with interconnected pores (pore diameter of 350 μm and interconnection diameter of 150 μm.

Parameter	Value
REV porosity	$\varepsilon \simeq 0.71$
REV volume	$V_{REV} \simeq 8$ mm^3
Permeability	$K = 2.1 \times 10^{-10}$ m^2
Relation between Q and u_D	$u_D = 0.727 \times 10^{-3}\ Q$
Optimal range of WSS	$\tau = [10^{-3.3}$Pa; $10^{-3.0}$Pa] (Section 2.4)
Optimal flow rate	$Q = 0.69$ mL · min^{-1}
Maximum growth rate of cell density	325% (7 days)

The Table 3 sums up the results for the different steps of the numerical protocol. The optimal range of WSS is identified thank to the computational protocol detailed in Section 2.4.

4. Discussion

The aim of our protocol is to predict cell growth inside a given macroporous scaffold put in a perfusion bioreactor. Cells are considered as osteoblasts and the scaffold is a 20 mm diameter and 20 mm high cylinder. Cell phenotype and scaffold dimensions are chosen to be consistent with our future standards in vitro analysis. The numerical protocol implementation needs several steps in which one or more key physical quantities are identified. By using a numerical protocol based on REV, the scaffold pore architecture is a critical design variable in the prediction of the development of cells. The size of our REV is close to analogue studies on perfusion inside porous media [53–57] i.e. around 5 to 10 mm^3.In several works a structured pores architecture is studied [53,55,56]. This could be relevant when using micro-structured arrangement of scaffold [58–64] but most of time scaffold are generally randomly structured. Our packing spheres generation based on random structures allows for variable use on both structured and unstructured internal architecture. However, another interesting approach is to use microCT scans to obtain the true internal architecture of porous media [1,65–67]. In this case, the CFD analysis could be more accurate than the one used in our protocol but the computational time and material used are much more expensive and nowadays difficult to value against standard clinical methods. The permeability identification step is used to link physical quantities like velocities and pressure at both microscale and macroscale. The method developed by Nugyen and colleagues [28] is capable to deal with any kind of porous material, even anisotropic scaffold, with full open porosity (spherical pores, foam, non-wooden structures. . .). Stress on full open porosity is a limit in our protocol but, in most cases, scaffolds are built in order to have a full open porosity to ensure whole cell colonization. The permeability identification step also shows the permeability as a function of inlet flow rate. The protocol is written for a permeability considered as a constant to validate our relation between microscale and macroscale via the Darcy Law. To keep permeability as a constant, velocities inside pores must not exceed 1.9 mm · s^{-1}. This value correspond to a pressure gradient of above 1000 Pa · m^{-1} which represents an inlet flow rate of our bioreactor of above 36 mL · min^{-1}. This is much greater than the values consistent with standard in vitro experiments i.e. between 0.1 and 10 mL · min^{-1} [1,53,65] and the hypothesis of a constant permeability is justified. The next step is the study of the Wall Shear Stress (WSS). Although the previous steps could be replaced by experimental analysis, at the present time, it is very difficult to carry out experimental measurements in porous media to identify Wall Shear Stress at microscale. Some 3D analysis [68,69] using Particle Image Velocimetry (PIV) are encouraging but need to be improved to complete with CFD studies. So, because it is not possible to measure the WSS experimentally, the optimal value of WSS for a given porous scaffold is not accurately known. Numerical studies are thus based on key quantities found in literature such as in Tab.1 to evaluate the optimal WSS.

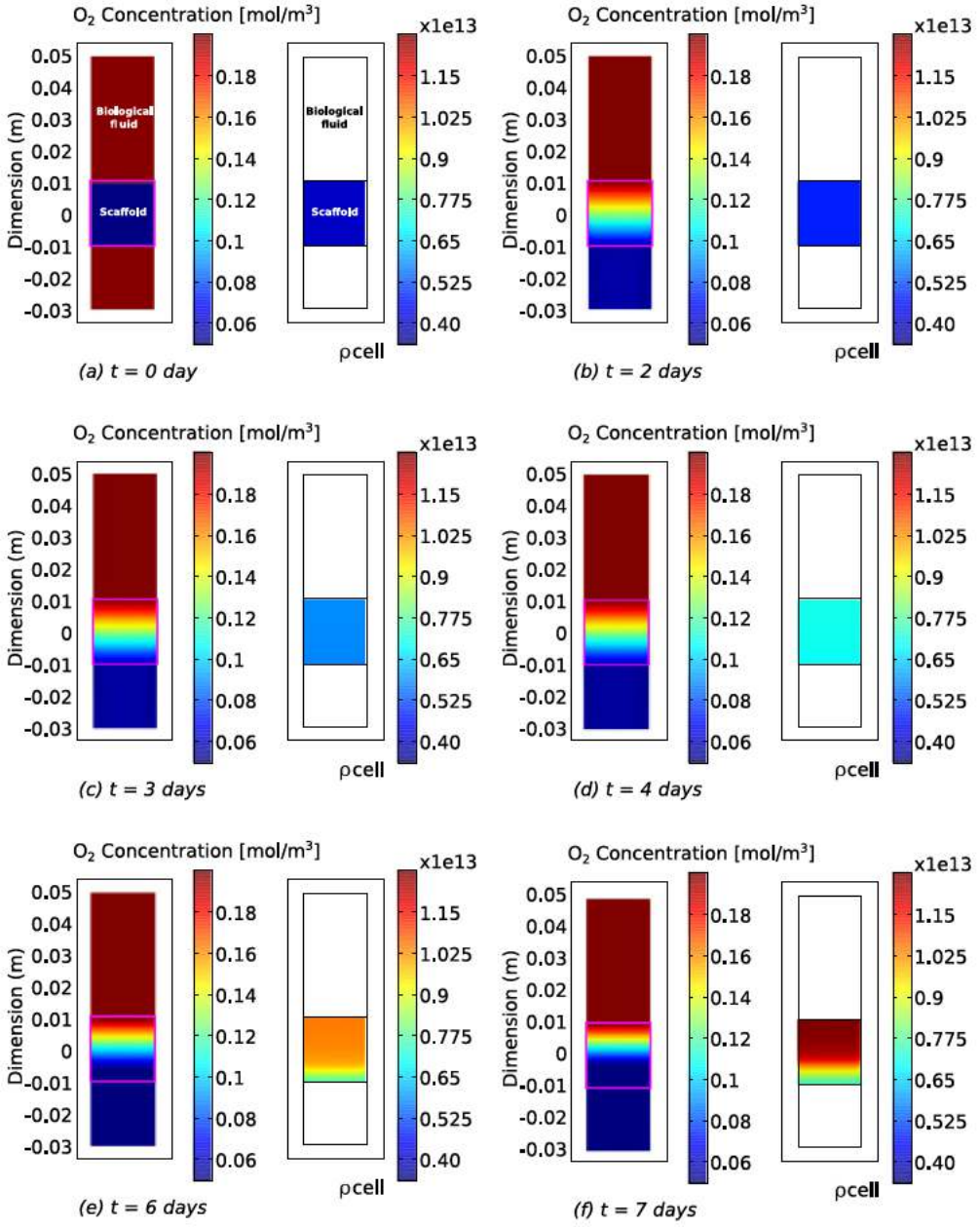

Fig. 9. Distribution of dioxygen concentration c_{O2} and number of cells ρ_{cell} inside the bioreactor for several time-step (initial time to 7 days).

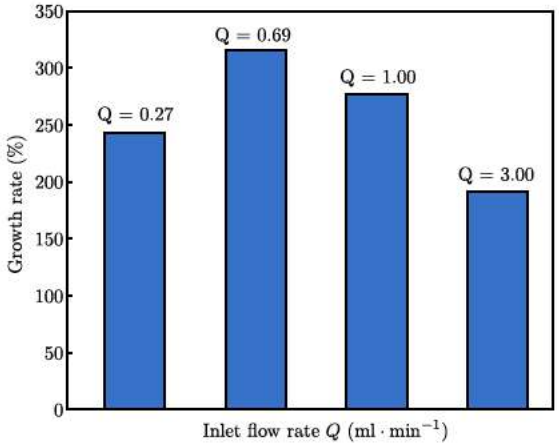

Fig. 10. Growth rate of cell colonization as a function of inlet flow rate after a 7-day-cell culture.

Without using microCT scan geometry models, two approaches are possible. The inlet flow rate can be imposed for several internal structured architectures [53] and then compared to find the scaffold into which the cell colonization is the highest. The strong point of this method is that it is easy to implement and identify the best scaffold for a given bioreactor. However, the default inlet flow rate is not necessary the best for cell growth and the same scaffold could produce better cell colonization with another inlet flow rate. Therefore, to find intermediate values, both inlet flow rate and internal architecture have to be considered during the WSS analysis such as proposed in our protocol. The computational time for our 190 tests is around a week on GPU station. The identified range of WSS (from 0.5 to 1 mPa) may be compared to other studies [53,55,65,68,70]. Once the WSS identified, and after a statistical analysis, a connection between microscale and macroscale is established. Any kind of external geometries (ie REV arrangements from cube to explicit representation of a bone) can be studied to evaluate and optimize the inlet flow rate inducing

the highest cell colonisation rate. In other words, for a given scaffold internal architecture and a given cell phenotype, only the last step of the protocol must be carried out (one day of computation) to identify an optimal inlet flow rate. In the final step, the nutrient diffusion is taken into account. This step is found in some studies evaluating cell growth [54,65,71–73]. Indeed, the identification of optimal range of WSS alone is not able to predict the cell proliferation rate for a given period of time because nutrient diffusion is not considered. Several studies have highlighted that oxygen concentration can be modelled and used to accurately predict cell growth rate [65,70–72]. As expected, the consumption of nutrient and consequently cell growth is higher at the top of the scaffold and a gradient of oxygen consumption is observed inside the scaffold. This main result using simulation is in accordance with in vitro tests [70,74,75] in which the gradient is observed. The information on cell growth is quantitative and shows an optimal colonization of 325% for a 7-day-cell culture for an inlet flow rate of 0.69 $mL \cdot min^{-1}$. The present model have some drawbacks such as the computational time for the first steps and its great dependence to porous architecture and cell phenotype that makes it necessary to carry out the entire protocol if another kind of scaffold or cell phenotype needs to be studied. The model requires that the cell type used be osteoblasts. Indeed, the choice of cell phenotype is a limitation of the model to ensure accuracy and predictability *in vitro* experiments. The cell type also significantly affects the *in vitro* results. In terms of accuracy in the description of hydrodynamic phenomena the model must be improved to take into account heterogeneous structures like foam with porosity gradient [76]. Furthermore, even if the model is able to consider the changes in porosity and permeability due to the cell growth, the consequent changes on Wall Shear Stress is not taken into account. This is a limitation of the model that can be solved by adding a new CFD step at the microscale between two optimisations at the macroscale. The new CFD step needs to rescale and to mesh again the pores assembly in order to evaluate the WSS distribution. This, however, requires a significant effort in terms of calculus costs. However, the major criticism of the model described in this paper is obviously the lack of experimental validation such as in vitro tests. The comparison between the model and *in vitro* tests will be produced in a future paper. The main aim of this paper is to clearly detail an entire numerical protocol and give the keys to adapt it to various cell cultures. In fact, for an alternative scenario, the parameters changes determine what part of the protocol must but carried out. If pores sizes and interconnexion change, all steps of the protocol need to be carried because of the impact of pores arrangement on permeability. If cell phenotype changes, the range of WSS must be reconsidered (determination of optimal range of WSS). The kind of bioreactor could also be consider to select a range of inlet flow rates (perfusion or rotating flow could be considered). The determination of the relation between WSS and Darcy velocities is the same for all scenarios. The optimal flow rate identification also depends on cell phenotype and mainly on oxygen consumption. On the mathematical models, others convection-diffusion laws can be added if needed. So, main parameters are pores arrangement, cell phenotype (needed stress and nutrients) and range of inlet flow rate that the bioreactor can provide.

As stated above in previous works [8,53,67,75,77,78] the determination of optimal flow conditions of a bioreactor "should be supported by simulation methods".

5. Conclusion

To conclude, our results show that an adapted protocol may be useful to preliminary tests instead of a trial-and-error approach. However, the computational protocol is built in a way that any part of the protocol could be replaced by experimental tests so as not to close the door to possible future experimental methods more suitable and easier to implement. The strong point of our method is its versatility.

Conflicts of interest

Authors declare no conflicts of interest.

Ethical approval

Not applicable

References

[1] McCoy R, Jungreuthmayer C, O'Brien F. Influence of flow rate and scaffold pore size on cell behavior during mechanical stimulation in a flow perfusion bioreactor. Biotechnol Bioeng 2012;109:1583–94.

[2] Farrell E, Byrne E, Fischer J, O'Brien F, O'Connell B, Prendergast P, et al. A comparison of the osteogenic potential of adult rat mesenchymal stem cells cultured in 2-D and on 3-D collagen glycosaminoglycan scaffolds. Technol Health Care 2007;15:19–31.

[3] Kim HJ, Kim UJ, Vunjak-Novakovic G, Min B, Kaplan D. Influence of macroporous protein scaffolds on bone tissue engineering from bone marrow stem cells. Biomaterials 2005;26:4442–52.

[4] Keogh M, O'Brien F, Daly J. Substrate stiffness and contractile behaviour modulate the functional maturation of osteoblasts on a collagen–gag scaffold. Acta Biomater 2010;6:4305–13.

[5] Morey E, Baylink D. Inhibition of bone formation during space flight. Science 1978;201:1138–41.

[6] Zerwekhand J, Ruml LA, Gottschalk F, Pak C. The effects of twelve weeks of bed rest on bone histology, biochemical markers of bone turnover, and calcium homeostasis in eleven normal subjects. J Bone Miner Res 1998;13:1594–601.

[7] Yu X, Botchwey E, Levine E, Pollack S, Laurencin C. Bioreactor-based bone tissue engineering: the influence of dynamic flow on osteoblast phenotypic expression and matrix mineralization. PNAS 2004;101(31):11203–8.

[8] Martin I, Wendt D, Heberer M. The role of bioreactors in tissue engineering. Trends Biotechnol 2004;22(2):80–6.

[9] Allori AC, Sailon AM, Clark E, Cretiu-Vasiliu C, Smay J, Ricci JL, et al. Dynamic cell culture for vascularized bone engineering. J Am Coll Surg 2008;207(3, Supplement):S51–2.

[10] da Silva HM, Mateescu M, Damia C, Champion E, Soares G, Anselme K. Importance of dynamic culture for evaluating osteoblast activity on dense silicon–substituted hydroxyapatite. Coll Surf B: Biointerfaces 2010;80(2):138–44.

[11] Plunkett NA, Partap S, O'Brien FJ. Osteoblast response to rest periods during bioreactor culture of collagenglycosaminoglycan scaffolds. Tissue Eng Part A Tissue Eng Part A 2010;16(3):943–51.

[12] Navarro F, Mizuno S, Huertas J, Julie G. Perfusion of medium improves growth of human oral neomucosal tissue constructs. Wound Repair Reg 2001;6:507–12.

[13] Goldstein AS, Juarez TM, Helmke CD, Gustin MC, Mikos AG. Effect of convection on osteoblastic cell growth and function in biodegradable polymer foam scaffolds. Biomaterials 2001;22(11):1279–88.

[14] Carrier R, Rupnick M, Langer R, Shoen F, Freed L, Vunjak-Novakovic G. Perfusion improve tissue architecture of engineered cardiac muscle. Tissue Eng 2002;8(2).

[15] Harris M, Doraiswamy A, Narayan R, Patz T, Chisey D. Recent progress in CAD/CAM laser direct-writing of biomaterials. Mater Sci Eng 2008;28(3):359–65.

[16] Olivier V, Hivart P, Descamps M, Hardouin P. In vitro culture of large bone substitutes in a new bioreactor: importance of the flow direction. Biomed Mater 2007;2(3):174.

[17] Hench L. Bioceramics: from concept to clinic. J Am Ceram Soc 1991;74(7):1487–510.

[18] Suchanek W, Yoshimura M. Processing and properties of hydroxyapatite-based biomaterials for use as hard tissue replacement implants. J Mater Res 1998;13:94–117.

[19] Luo E, Hu J, Bao C, Li Y, Tu Q, Murray D. Sustained release of adiponectin improves osteogenesis around hydroxyatite implants by suppressing osteoblast activity in ovariectomized rabbits. Acta Biomater 2012;8(2):734–43.

[20] Lee J, Jang H, Lee K, Baek H, Jin K, Hong K. In vitro and in vivo evaluation of the bioactivity of hydroxyapatite-coated polyetheretherketone biocomposites created by cold spray technology. Acta Biomater 2013;9(4):6177–87.

[21] Wen C, Xu W, Hu W, Hodgson P. Hydroxyapatite/titania solgel coating on titaniumzirconium alloy for biomedical applications. Acta Biomater 2009;3(3):403–10.

[22] Lakstein D, Kopelovitch W, Barkay Z, Bahaa M, Hendel D, Heliaz N. Enhanced osseointegration of grit-blasted, NaOH-treated and electrochemically hydroxyapatite-coated ti6al4v implants in rabbits. Acta Biomater 2009;5(6):2258–69.

[23] Wang W, Itoh S, Tanaka Y, Nagai A, Yamashita K. Comparison of enhanced of bone ingrowth into hydroxyapatite ceramics with highly and poorly interconnected pores by electrical polarization. Acta Biomater 2009;5(8):3132–40.

[24] Davisson T, Sah R, Ratcliffe A. Perfusion increases cell content and matrix synthesis in chondrocyte three-dimensional cultures. Tissue Eng 2004;8(5):807–16.
[25] Jungreuthmayer C, Donahue S, Jaasma M, Al-Munajjed A, Zanghellini J, Kelly D, et al. A comparative study of shear stresses in collagen-glycosaminoglycan and calcium phosphate scaffolds in bone tissue-engineering bioreactors. Tissue Eng 2008;15(5):1141–9.
[26] Descamps M, Duhoo T, Monchau F, Lu J, Hardouin P, Hornez J, et al. Synthesis of macroporous beta-tricalcium phosphate with controlled porous architectural. Ceram Int 2008;34:1131–7.
[27] Millman K, Jarrod K, Aivazis M. Python for scientists and engineers. Comput Sci Eng 2011;13(2):9–12.
[28] Nugyen T-K, Carpentier O, Herin P, Hivart P. Numerical approach of the permeability of a macroporous bioceramic with interconnected spherical pores. Transp Porous Media 2013;96 (2):255–70.
[29] Zhao F, Chella R, Ma T. Effects of shear stress on 3-D human mesenchymal stem cell construct development in a perfusion bioreactor system: experiments and hydrodynamic modeling. Biotechnol Bioeng 2007;96(3):584–95.
[30] Porter B, Zauel R, Stockman H, Guldberg R, Fyhrie D. 3-D computational modeling of media flow through scaffolds in a perfusion bioreactor. J Biomech 2005;38(3):543–9.
[31] Raimondi MT, Moretti M, Cioffi M, Giordano C, Boschetti F, Laganà K, et al. The effect of hydrodynamic shear on 3D engineered chondrocyte systems subject to direct perfusion. Biorheology 2006;43(3):215–22.
[32] Xu S, Li D, Xie Y, Lu J, Dai K. The growth of stem cells within beta-TCP scaffolds in a fluid-dynamic environment. Mater Sci Eng: C 2008;28(1):164–70.
[33] Li D, Tang T, Lu J, Dai K. Effects of flow shear stress and mass transport on the construction of a large-scale tissue-engineered bone in a perfusion bioreactor.. Tissue Eng Part A 2009;15(10):2773–83.
[34] Sandino C, Planell J, Lacroix D. A finite element study of mechanical stimuli in scaffolds for bone tissue engineering. J Biomech 2008;41(5):1005–14.
[35] YJia, Bagnaninchi P, Yang Y, El Haj A, Hinds M, Kirkpatrick S, et al. Doppler optical coherence tomography imaging of local fluid flow and shear stress within microporous scaffolds. J Biomed Opt 2009;14(3): 034014.
[36] Campos M, Grossi T, Bianchi E, Dubini G, Lacroix D. 2D μ-particle image velocimetry and computational fluid dynamics study within a 3D porous scaffold.. Ann Biomed Eng 2017;45(5):1341–51.
[37] Powell M. An efficient method for finding the minimum of a function of several variables without calculating derivatives. Comput J 1964;7(2):155–62.
[38] Obradovic B, Meldon JH, Freed LE, Vunjak-Novakovic G. Glycosaminoglycan deposition in engineered cartilage: experiments and mathematical model. AIChE J 2000;46(9):1860–71.
[39] Haselgrove JC, Shapiro IM, Silverton SF. Computer modeling of the oxygen supply and demand of cells of the avian growth cartilage. Am J Physiol - Cell Physiol 1993;265(2):C497–506.
[40] Coletti F, Macchietto S, Elvassore N. Mathematical modeling of three--dimensional cell cultures in perfusion bioreactors. Ind Eng Chem Res 2006;45(24):8158–69.
[41] Galban CJ, Locke BR. Analysis of cell growth kinetics and substrate diffusion in a polymer scaffold. Biotechnol Bioeng 1999;65(2):121–32.
[42] Chung C, Chen C, Chen C, Tseng C. Enhancement of cell growth in tissue-engineering constructs under direct perfusion: modeling and simulation. Biotechnol Bioeng 2007;97(6):1603–16.
[43] Gosgnach W, Messika-Zeitoun D, Gonzalez W, Philipe M, Michel J-B. Shear stress induces INOS expression in cultured smooth muscle cells: role of oxidative stress. Am J Physiol - Cell Physiol 2000;279(6):C1880–8.
[44] Richardson RS. Oxygen transport and utilization: an integration of the muscle systems. Adv Physiol Educ 2003;27(4):183–91.
[45] Wagner B, Venkataraman S, Buettner G. The rate of oxygen utilization by cells. Free Rad Biol Med 2011;51(3):700–12.
[46] Herst P, Berridg M. Cell surface oxygen consumption: a major contributor to cellular oxygen consumption in glycolytic cancer cell lines. Biochim Biophys Acta (BBA) - Bioenerg 2007;1767(2):170–7.
[47] Grover W., Bryan A., Diez-Silva M., Suresh S., Higgins J., Manalis S.. Measuring single-cell density. Proceedings of the National Academy of Sciences2011.
[48] Burg T, Godin M, Knudsen S, Shen W, Carlson G, Foster J, et al. Weighing of biomolecules, single cells and single nanoparticles in fluid. Nature 2007;446:1066–9.
[49] Docheva D, Padula D, Popov C, Mutschler W, Clausen-Schaumann H, Schieker M. Researching into the cellular shape, volume and elasticity of mesenchymal stem cells, osteoblasts and osteosarcoma cells by atomic force microscopy. J Cell Molec Med 2008;12(2):537–52.
[50] Landman K, Cai A. Cell proliferation and oxygen diffusion in a vascularising scaffold. Bull Math Biol 2007;69:2405–28.
[51] Croll TI, Gentz S, Mueller K, Davidson M, O'Connor AJ, Stevens GW, et al. Modelling oxygen diffusion and cell growth in a porous, vascularising scaffold for soft tissue engineering applications. Chem Eng Sci 2005;60(17):4924–34.
[52] Zhu Z, Wang Q, Wu Q. On the examination of the Darcy permeability of soft fibrous porous media; new correlations. Chem Eng Sci 2017;173:525–36.
[53] Boschetti F, Raimondi M, Migliavacca F, Dubini G. Prediction of the micro-fluid dynamic environment imposed to three-dimensional engineered cell systems in bioreactors. J Biomech 2006;39:418–25.
[54] Tourlomousis F, Chang R. Numerical investigation of dynamic microorgan devices as drug screening platforms. part ii: microscale modeling approach and validation. BiotechnolBioeng 2015;113(3):623–34.
[55] Lacroix D, Planell J, Prendergast P. Computer-aided design and finite-element modelling of biomaterial scaffolds for bone tissue engineering. Philos Trans Royal Soc A 2009;367:1993–2009.
[56] Sanz-Herrera J, Garcia-Aznar J, Doblare M. On scaffold designing for bone regeneration: a computational multiscale approach. Acta Biomater 2009;5:219–29.
[57] Freitas D, Almeida H, Bartolo P. Perfusion bioreactor fluid flow optimization. Proc Technol 2014;16:1238–47.
[58] Takagi K, Takahashi T, Kikuchi K, Kawasaki A. Fabrication of bioceramic scaffolds with ordered pore structure by inverse replication of assembled particles. J Eur Ceram Soc 2010;30(10):2049–55.
[59] Tan J, Chua C, Leong K. Fabrication of channeled scaffolds with ordered array of micro-pores through microsphereleaching and indirect rapid prototyping technique. Biomed Microdev 2012;15:1–14.
[60] Wang X, Xu S, Zhou S, Xu W, Leary M, Choong P, et al. Topological design and additive manufacturing of porous metals for bone scaffolds and orthopaedic implants: a review. Biomaterials 2016;83:127–41.
[61] Mohanty S, Sanger K, Heiskanen A, Trifol J, Szabo P, Dufva M. Fabrication of scalable tissue engineering scaffolds with dual-pore microarchitecture by combining 3D printing and particle leaching. Mater Sci Eng C 2016;61:180–9.
[62] Cavo M, Scaglione S. Scaffold microstructure effects on functional and mechanical performance: integration of theoretical and experimental approaches for bone tissue engineering applications. Mater Sci Eng C 2016;68:872–9.
[63] An J, Teoh J, Suntornnond R, Chua C. Design and 3D printing of scaffolds and tissues. Engineering 2015;1(2):261–8.
[64] Munaz A, Vadilevu R, St John J, Barton M, Kamble H. Three-dimensional printing of biological matters. J Sci: Adv Mater Dev 2016;1:1–17.
[65] Grayson W, Marolt D, Bhumiratana S, Fröhlich M, Guo E, Vunjak-Novakovic G. Optimizing the medium perfusion rate in bone tissue engineering bioreactors. Biotechnol Bioeng 2011;108(5):1159–70.
[66] Andreaus U, Colloca M, Iacoviello D. Optimal bone density distributions: numerical analysis of the osteocyte spatial influence in bone remodeling. Comput Methods Programs Biomed 2014;113:80–91.
[67] Costantini M, Colosi C, Mozetic P, Jaroszewicz J, Tosato A, Rainer A, et al. Correlation between porous texture and cell seeding efficiency of gas foaming and microfluidic foaming scaffolds. Mater Sci Eng C 2016;62:668–77.
[68] Mack J, Youssef K, Noel O, Lake M, Wu A, Luisa Iruela-Arispe M, et al. Real-time maps of fluid flow fields in porous biomaterials. Biomaterials 2012;34(8):1980–6.
[69] Xu S. Study on flow field in new bioreactor by PIV in lower onflow state. Procedia Eng 2012;29:3939–43.
[70] Ferroni M, Giusti S, Nascimento D, Silva A, Boschetti F. Modeling the fluid–dynamics and oxygen consumption in a porous scaffold stimulated by cyclic squeeze pressure. Med Eng Phys 2016;38:725–32.
[71] Santoro R, Krause C, Martin I, Wendt D. On-line monitoring of oxygen as a non-destructive method to quantify cells in engineered 3D tissue constructs. J Tissue Eng Regen Med 2012;6:696–701.
[72] Yu P, Lee T, Zeng Y, Low H. A 3D analysis of oxygen transfer in a low-cost micro-bioreactor for animal cell suspension culture. Comput Methods Programs Biomed 2007;85:59–68.
[73] Patrachari A, Podichetty J, Podichetty T, Madihally S. Application of computational fluid dynamic in tissue engineering. J Biosci Bioeng 2012;114(2):123–32.
[74] Bergemann C, Elter P, Lange R, Weißmann V, Hansmann H, Klinkenberg E, et al. Cellular nutrition in complex three-dimensional scaffolds: a comparison between experimentsand computer simulations. Int J Biomater 2015;2015:1–12.
[75] Sinlapabodin S, Damrongsakkul PAS, Kanokpanont S. An axial distribution of seeding, proliferation, and osteogenic differentiation of mc3t3-e1 cells and rat bone marrow-derived mesenchymal stem cells across a 3d thai silk fibroin/gelatin/hydroxyapatite scaffold in a perfusion bioreactor. Mater Sci Eng C 2016;58:960–70.
[76] Miao X, Sun D. Graded/gradient porous biomaterials. Materials 2010;3:26–47.
[77] Sun W, Lal P. Recent development on computer aided tissue engineering - a review. Comput Methods Programs Biomed 2002;67:85–103.
[78] Liu Y, Lu H. Microfluidics in systems biology – hype or truly useful? Curr Opin Biotechnol 2016;39:215–20.